

# Spectral effective emissivities of nonisothermal cavities calculated by the Monte Carlo method

V. I. Sapritsky and A. V. Prokhorov

An algorithm based on the Monte Carlo method is described that permits the precise calculation of radiant emission characteristics of nonisothermal blackbody cavities for use as standard sources in radiometry, photometry, and radiation thermometry. The algorithm is realized for convex axisymmetric specular-diffuse cavities formed by three conical surfaces. The numerical experiments provide estimates of normal effective emissivities of cylindrical blackbody cavities with flat or conical bottoms for various axisymmetric temperature distributions on the cavity walls.

## 1. Introduction

Blackbody cavities are widely used as standard sources in radiometry and spectroradiometry of noncoherent optical radiation, from the ultraviolet to the far infrared, and in radiation thermometry. Ideally, such a cavity should have isothermal walls at some temperature  $T_0$  and a small outlet for radiation to escape. Spectral characteristics of the radiation from the cavity can be calculated by the use of Planck's law, with the spectral effective emissivity of the cavity taken as a correction factor for disturbances from thermodynamic equilibrium.

In accordance with the extended Kirchhoff law for isothermal cavities<sup>1</sup> and the reciprocity theorem, and provided that the cavity walls are opaque, we can write

$$\epsilon_{e0}(\lambda, \xi, \omega) = \alpha_{e0}(\lambda, \xi, -\omega) = 1 - \rho_{e0}(\lambda, \xi, -\omega), \quad (1)$$

where  $\epsilon_{e0}$ ,  $\alpha_{e0}$ , and  $\rho_{e0}$  are the effective emissivity, absorptivity, and reflectivity of the isothermal cavity, respectively;  $\lambda$  is the wavelength;  $\xi$  is the radius vector to the cavity inner surface; and  $\omega$  is the direction of observation. Equation (1) makes it possible, in principle, for one to check experimentally the calculated effective emissivities of isothermal cavities by measuring their effective reflectivities with appropriate exposure conditions.

In fact, one cannot reach the ideal isothermality of the cavity walls, and a nonuniform temperature distribution on the emitting surface results in ambiguity in the reference temperature,  $T_0$ . For example, if the selected reference temperature is below the lowest temperature on the cavity walls, then all spectral effective emissivity values of the nonisothermal cavity,  $\epsilon_e(\lambda, \xi, \omega, T_0)$ , will exceed unity.

Because there are no direct methods for measuring the effective emissivities of nonisothermal cavities, it is necessary to develop independent methods of calculation to permit accurate corrections to be made for cavity geometry, spectral and angular functions of optical characteristics of the cavity walls, observation conditions, and other factors.

For diffuse cavities (i.e., cavities whose inner surfaces radiate and reflect in accordance with the Lambert cosine law), one can find the distribution of the local effective emissivities on the walls by solving the integral equations for radiation heat exchange. Numerical solutions for conical, cylindrical, cylindroconical, and biconical cavities have been obtained<sup>2-4</sup> by the use of the zonal approximation of the integrals and the iteration technique to solve the resultant system of linear equations. A cylinder with a reentrant conical base featuring mutual shadowing of the inner surfaces has been investigated in a similar manner.<sup>5</sup> The iterative procedure and finite-difference approximation of iterated kernels have been used<sup>6</sup> for calculating the effective emissivities of nonisothermal diffuse cavities of the classic geometrical shapes.

Although one can calculate the effective emissivities of nonisothermal, nondiffuse cavities by summing up contributions of successive radiation reflections, the complexity of the calculation of the multiple

The authors are with the Russian Research Institute for Optical and Physical Measurements (VNIIOFI), Ozernaya Street 46, Moscow 119361, Russia.

Received 12 September 1994; revised manuscript received 9 February 1995.

0003-6935/95/255645-08\$06.00/0.

© 1995 Optical Society of America.

integrals causes one either to correct for only two reflections<sup>7</sup> or to approximate distributions of reflected flows on the cavity walls by their average values.<sup>8</sup> Such simplifications may result in uncontrollable errors in the calculation.

As computer facilities are continuously being improved, the Monte Carlo method is used more and more frequently. It offers such advantages as the same approach to problems with various geometries, the possibility of correcting for real angular distributions of radiation flows, and the efficient and simple correction of the initial mathematical model. Among the modifications of the Monte Carlo method as applied for the calculation of cavity radiation characteristics, one can select algorithms based on either the geometric and probability approach<sup>9</sup> or on the energy approach.<sup>10</sup> The former uses a random particle walk in the cavity to estimate the probability of certain events (e.g., escape of a particle from the cavity after a certain combination of specular and diffuse reflections) in order to calculate emissivities of isothermal cavities. The latter deals with random trajectories along which radiation having certain energy characteristics is propagated, and it can be applied to nonisothermal cavities.

We discuss a modification of the Monte Carlo method that uses the geometric and probability approach to calculate radiation characteristics of isothermal cavities and the energy approach to calculate corrections for nonisothermal conditions.<sup>11</sup> An algorithm is described that ensures a reduced dispersion in the calculated value. It has been applied to a variety of axisymmetric cavities.

## 2. Analysis Restrictions

The cavities for the calculations were axisymmetric and coaxial, and they were formed by three conical surfaces (Fig. 1). By varying the linear and angular dimensions one can cover a variety of geometrical configurations, including simple shapes such as cones, cylinders, and double cones.

It is assumed that the walls of the cavity are opaque and that their optical characteristics are constant on

the whole inner surface and are temperature independent within the range from the lower temperature-distribution boundary to the upper one. The cavity inner surface is assumed to radiate diffusely with a spectral emissivity  $\epsilon(\lambda)$ , i.e., Lambert's cosine law is valid for the self-radiation intensity.

In accordance with Kirchhoff's law,

$$\epsilon(\lambda) + \rho(\lambda) = 1, \quad (2)$$

where  $\rho(\lambda)$  is the spectral reflectivity. Reflections from the cavity walls are described by a uniform specular-diffuse model,<sup>9</sup> according to which the spectral reflectivity,  $\rho(\lambda)$ , does not depend on the radiation incidence angle and is a sum of specular components,  $\rho_s(\lambda)$ , and diffuse components,  $\rho_d(\lambda)$ . Surface diffusivity, defined as

$$D = \frac{\rho_d(\lambda)}{\rho(\lambda)}, \quad (3)$$

is constant within the wavelength range under consideration, from  $\lambda_1$  to  $\lambda_2$ . Polarization effects can be ignored by the assumption that the radiation is depolarized after multiple reflections.

## 3. Calculation Algorithm

The effective spectral radiance of the radiation from the cavity aperture can be written as

$$L_e(\lambda, \xi, \omega) = \epsilon_e(\lambda, \xi, \omega, T_0)L_{BB}(\lambda, T_0), \quad (4)$$

where  $\lambda$  is the wavelength,  $\xi$  is the radius vector of the radiating surface point,  $\omega$  is the direction of observation,  $T_0$  is the reference temperature,  $\epsilon_e$  is the spectral effective emissivity of the nonisothermal cavity, and  $L_{BB}$  is the blackbody spectral radiance. It is obvious that specifying different  $T_0$  values for the same radiance being measured,  $L_e$ , will result in different functions,  $\epsilon_e$  and  $L_{BB}$ .

Let us represent  $\epsilon_e$  by the following equation:

$$\epsilon_e(\lambda, \xi, \omega, T_0) = \epsilon_{e0}(\lambda, \xi, \omega) + \Delta\epsilon_e(\lambda, \xi, \omega, T_0), \quad (5)$$

where the first term on the right-hand side represents the spectral effective emissivity of the isothermal cavity, whereas the second term is a correction for nonisothermal conditions.

We briefly describe the Monte Carlo algorithm for the calculation of the effective emissivities of isothermal cavities based on Eq. (1). The incident radiation is considered to consist of a rather large number of particles (photon bundles). Initially each particle is assigned a statistical weight of unity. A particle is incident upon the aperture from the point of observation outside the cavity in the direction of observation, and it interacts with the wall. After that, the radius vector of the first interaction point,  $\xi_1$ , is found. To determine the type of the interaction, we select a pseudorandom number,  $H_d$ , from the general population that is uniformly distributed on the interval (0, 1); the reflection is considered diffuse if  $H_d < D$  and is specular otherwise. In the event that reflec-

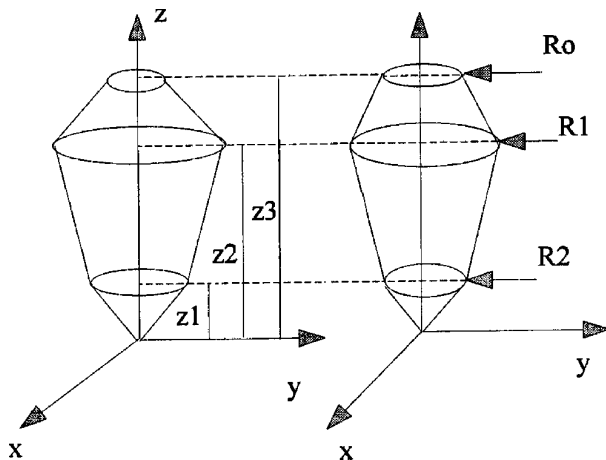


Fig. 1. Cavities to which the calculation is applied.

tion is specular, the statistical weight of the particle is  $z = z' + \omega_z t$  transformed as follows: (14)

$$W = \rho(\lambda)W', \quad (6)$$

where  $W'$  and  $W$  are the statistical weights before and after reflection, respectively.

When the reflection is specular, unit vectors describing the directions of incidence,  $\omega'$ , and reflection,  $\omega$ , are related by the following equation:

$$\omega = \omega' - 2n(n\omega), \quad (7)$$

where  $n$  is the inner, unit-length, normal vector to the cavity surface at the point of interaction. If the reflection is diffuse then the diffuse angle factor,  $F(\xi)$ ,<sup>12</sup> must be calculated between the surface element at the point of interaction,  $\xi$ , and the cavity aperture:

$$F(\xi) = \left(\frac{1}{\pi}\right) \int_{\Omega} \cos \theta_{\xi} d\Omega, \quad (8)$$

where  $\Omega$  is the solid angle subtended by the aperture from the point  $\xi$ , and  $\theta_{\xi}$  is the angle between the normal to the cavity wall at point  $\xi$  and the axial direction of the elementary solid angle,  $\Omega$ . The statistical weight of the particle can be transformed by the use of the following formula:

$$W = \rho(\lambda)[1 - F(\xi)]W'. \quad (9)$$

If the first reflection is diffuse, then the method of trajectory splitting is used: the particle gives birth to  $n_0$  descendants, each one having a statistical weight of  $W/n_0$  and continuing random walks along its trajectories. Optimum value  $n_0$  should be found empirically and can be estimated to be  $1/(1 - \epsilon_e)^{0.5}$ . For the majority of practical blackbodies,  $n_0 = 10-100$ . In the event of diffuse reflection, the direction of particle reflection is determined randomly. Two regular random numbers,  $H_{\theta}$  and  $H_{\phi}$ , are transformed into angular coordinates,  $\theta$  and  $\Psi$ , of the spherical system with the center at the point of reflection<sup>12</sup>:

$$\theta = \arcsin \sqrt{H_{\theta}}, \quad (10)$$

$$\phi = 2\pi H_{\phi}. \quad (11)$$

These in turn are transformed into components of the normal vector,  $\omega$ .

After finding the direction of particle movement,  $\omega$  with  $\omega_x$ ,  $\omega_y$ , and  $\omega_z$  components, one can calculate the  $x$ ,  $y$ ,  $z$  components of the radius vector of a regular particle interaction with the cavity wall,  $\xi$ , on the basis of a joint solution of the following parametric equations of the particle trajectory,

$$x = x' + \omega_x t, \quad (12)$$

$$y = y' + \omega_y t, \quad (13)$$

(primed coordinates are related to the point of previous interaction) and the following cavity surface equation:

$$x^2 + y^2 - (z - z_{0i})^2 \tan^2(\chi_i/2) = 0. \quad (15)$$

Here  $z_{0i}$  are coordinates of the vertices of the conical surfaces forming a cavity,  $\chi_i$  are the angles at these vertices (see Fig. 1), and

$$\begin{aligned} i = 1 & \quad \text{with } 0 < z < z_1, \\ & = 2 \quad \text{with } z_1 < z < z_2, \\ & = 3 \quad \text{with } z_2 < z < z_3. \end{aligned}$$

If the particle leaves the cavity after a diffuse reflection then the last trajectory is ignored, because the weight of the particle that left was already taken into account by means of the diffuse angle factor. Thus the particle trajectory ends if either the particle leaves the cavity as a result of a specular reflection or the descendant particle has a statistical weight of less than a certain prespecified value, defining the appropriate nonexcluded error.

The statistical modeling ends when the necessary number of trajectory realizations,  $n$ , is reached. The cavity effective emissivity can be estimated by means of the following formula:

$$\begin{aligned} \epsilon_e(\lambda, \xi, \omega) = 1 - & \left(\frac{1}{nn_0}\right) \sum_{i=1}^n \sum_{j=1}^{n_{0i}} \sum_{k=1}^{m_{ij}} \rho^k(\lambda) F(\xi_{ijk}) \\ & \times \prod_{l=1}^{k-1} [1 - F(\xi_{ijl})], \quad (16) \end{aligned}$$

where  $n_{0i} = n_0$  for the first diffuse reflection,  $n_{0i} = 1$  for the first specular reflection,  $\xi_{ijk}$  is the radius vector of the  $k$ th reflection of the  $j$ th descendant of the  $i$ th particle, and  $m_{ij}$  is the number of reflections in the trajectory of the  $j$ th descendant of the  $i$ th particle. In the event of specular reflection,  $F(\xi) = 1$  if the particle leaves the cavity through the aperture; otherwise,  $F(\xi) = 0$ .

To calculate the effective emissivity of the nonisothermal cavity, we make use of the reciprocity theorem and the same particle trajectories as when we calculate the effective emissivity of the isothermal cavity. By calculating the spectral radiance,  $L_{BB}$ , at a wavelength of  $\lambda$  and at temperature  $T_{ijk}$  of the cavity surface at the point of interaction, and by summing up their products into appropriate degrees  $\rho(\lambda)$ , we can obtain the following estimate of the effective spectral radiance:

$$L_e(\lambda, \xi, \omega) = \frac{\epsilon(\lambda)}{nn_0} \sum_{i=1}^n \sum_{j=1}^{n_{0i}} \sum_{k=1}^{m_{ij}} \rho^{k-1}(\lambda) L_{BB}(\lambda, T_{ijk}) \gamma_{ijk}, \quad (17)$$

where  $T_{ijk}$  is the temperature of the cavity surface at

the point of the  $k$ th reflection of the  $j$ th descendant of the  $i$ th particle, and  $\gamma_{ijk} = 1$  until the next diffuse direction passes through the cavity aperture, after which  $\gamma_{ijk} = 0$ .

From Eqs. (4) and (17) we have

$$\epsilon_e(\lambda, \xi, \omega, T_0) = \frac{\epsilon(\lambda)}{nn_0 L_{BB}(\lambda, T_0)} \sum_{i=1}^n \sum_{j=1}^{n_{0i}} \sum_{k=1}^{m_{ij}} \rho^{k-1}(\lambda) L_{BB}(\lambda, T_{ijk}) \gamma_{ijk}. \quad (18)$$

For isothermal cavity  $T_{ijk} = T_0$ , therefore, the estimated effective emissivity of the isothermal cavity is obtained from Eq. (18) as follows:

$$\epsilon_{e0}(\lambda, \xi, \omega) = \frac{\epsilon(\lambda)}{nn_0} \sum_{i=1}^n \sum_{j=1}^{n_{0i}} \sum_{k=1}^{m_{ij}} \rho^{k-1}(\lambda) \gamma_{ijk}. \quad (19)$$

The numerical experiments performed have shown that, when all other conditions are equal, the algorithm described by Eq. (16) provides a 2–3 times decrease in the standard deviation as compared with that described by Eq. (19). For that reason, a combined algorithm is used:  $\epsilon_{e0}(\lambda, \xi, \omega)$  is estimated according to Eq. (16), whereas  $\Delta\epsilon_e(\lambda, \xi, \omega)$  is derived from Eq. (18).

By subtracting Eq. (19) from Eq. (18) we obtain

$$\Delta\epsilon_e(\lambda, \xi, \omega, T_0) = \frac{\epsilon(\lambda)}{nn_0 L_{BB}(\lambda, T_0)} \sum_{i=1}^n \sum_{j=1}^{n_{0i}} \sum_{k=1}^{m_{ij}} \rho^{k-1}(\lambda) \times [L_{BB}(\lambda, T_{ijk}) - L_{BB}(\lambda, T_0)] \gamma_{ijk}. \quad (20)$$

By summing up Eq. (16) and Eq. (20) for the combined algorithm we obtain

$$\epsilon_e(\lambda, \xi, \omega, T_0) = 1 + \frac{1}{nn_0} \sum_{i=1}^n \sum_{j=1}^{n_{0i}} \sum_{k=1}^{m_{ij}} \left\{ \frac{\rho^{k-1}(\lambda) \epsilon(\lambda) [L_{BB}(\lambda, T_{ijk}) - L_{BB}(\lambda, T_0)] \gamma_{ijk}}{L_{BB}(\lambda, T_{ijk})} - \rho(\lambda) F(\xi_{ijk}) \prod_{l=1}^{k-1} [1 - F(\xi_{il})] \right\}. \quad (21)$$

Thus, the algorithm described above represents the modeling of a great number of trajectories splitting at the point of the first reflection (if it is diffuse), the calculation of diffuse angle factors and spectral radiances at reflection points, and the calculation of effective emissivities determined according to Eq. (21).

The normal effective emissivity,  $\epsilon_{en}$ , is important in practical precise radiometry. To calculate it, one models the initial trajectory sections to be parallel to the plane axis and to be uniformly distributed on the aperture cross section. For evaluation of the accuracy of the proposed algorithm with  $n = 1000$  and  $n_0 = 20$ , the calculations of the normal effective emissivities of diffuse cavities described in Refs. 2, 4, and 6 have been executed. For isothermal cavities

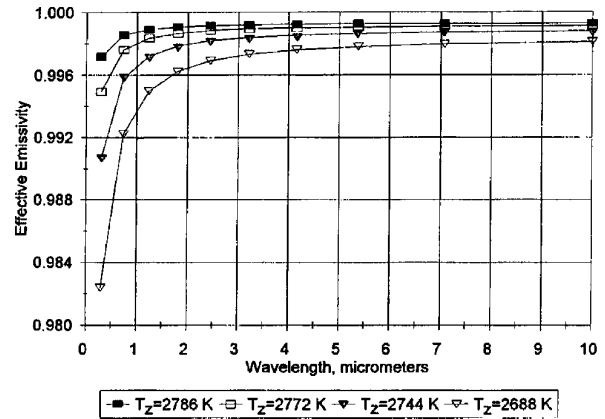


Fig. 2. Spectral normal effective emissivities of a cylindrical cavity for the first family of temperature distributions.

with  $\epsilon_{e0n} > 0.9$  the divergence does not exceed 0.0001, and for nonisothermal cavities with  $|1 - \epsilon_{en}| < 0.1$  the divergence is equal to 0.0001–0.0004. A comparison with the results for isothermal specular-diffuse cavities considered in Ref. 9 has shown good agreement with our results.

#### 4. Cylindrical Cavity with Flat Bottom

The object for the numerical experiments was a cylindrical graphite cavity with a flat bottom and a flat diaphragm, having the following geometric parameters: aperture radius  $R_0 = 0.5$ , cylinder radius  $R_0 = 1$ , and cavity length  $Z_3 = 10$  (parameters are given in relative units). Within the spectral region of 0.3 to 10  $\mu\text{m}$ , the cavity inner surface is diffuse ( $D = 1$ ) and has constant emissivity  $\epsilon(\lambda) = 0.8$ . Spectral normal effective emissivities for six families of temperature distributions on the cavity generatrix have been computed.

For the first family of temperature distributions it

was assumed that the bottom of the cavity and the adjacent three quarters of the cylindrical generatrix were isothermal at a temperature of 2800 K, and that there was a linear decrease to temperature  $T_z$  (2786, 2772, 2744, and 2688 K) in the edge of the cylindrical part of the cavity (see Fig. 2).

For the second family of temperature distributions it was assumed that the bottom and the adjacent half of the cylindrical generatrix were isothermal at a temperature of 2800 K, and that there was a linear decrease to temperature  $T_z$  in the other cylindrical part (temperatures were the same; see Fig. 3).

For the third family of temperature distributions it was assumed that the bottom and the adjacent quarter of the cylindrical generatrix were isothermal at a temperature of 2800 K, and that there was a linear

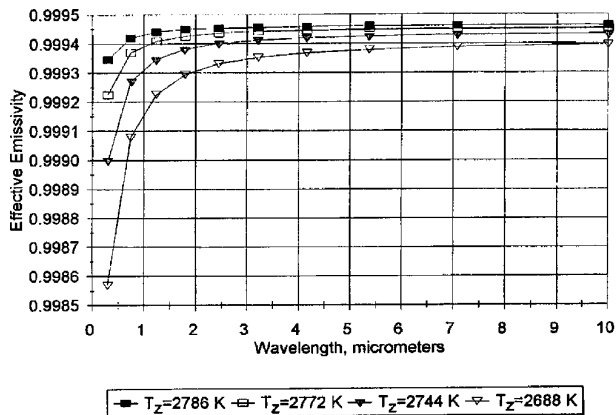


Fig. 3. Spectral normal effective emissivities of a cylindrical cavity for the second family of temperature distributions.

decrease to temperature  $T_z$  in the other three quarters of the cylindrical generatrix (temperatures were the same; see Fig. 4).

For the fourth family of temperature distributions it was assumed that the bottom of the cavity was isothermal at a temperature of 2800 K, and that there was a linear decrease to temperature  $T_z$  in the edge of the cylindrical part (temperatures were the same; see Fig. 5).

For the fifth family of temperature distributions it was assumed that the bottom center temperature was 2800 K, there was a linear increase to temperature  $T_z$  to the bottom periphery (2801, 2802, 2803, and 2804 K), and that the rest of the cavity was isothermal at temperature  $T_z$  (see Fig. 6).

For the sixth family of temperature distributions it was assumed that the bottom center temperature was 2800 K, there was a linear decrease to temperature  $T_z$  to the bottom periphery (2799, 2798, 2793, and 2786 K), and that the rest of the cavity was isothermal at temperature  $T_z$  (see Fig. 7).

In each of the above cases the bottom center temperature (equal to 2800 K) was taken as a reference temperature, and the diaphragm of the cavity was isothermal at the temperature  $T_z$ . Spectral normal effective emissivities calculated for the above

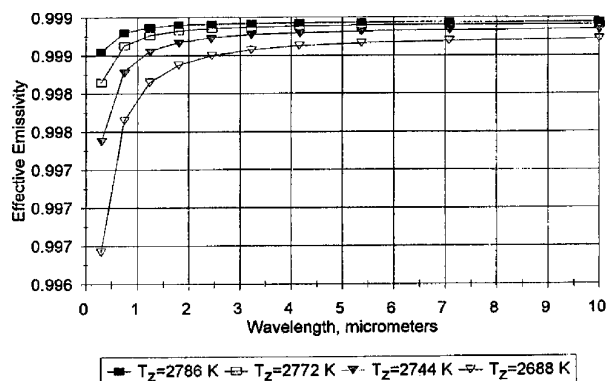


Fig. 4. Spectral normal effective emissivities of a cylindrical cavity for the third family of temperature distributions.

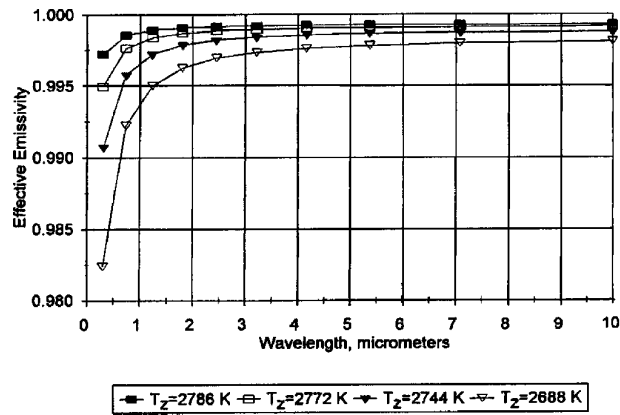


Fig. 5. Spectral normal effective emissivities of a cylindrical cavity for the fourth family of temperature distributions.

six families of temperature distributions are given in Figs. 2-7, respectively.

### 5. Cylindrical Cavity with Conical Bottom

The numerical experiments have also been carried out for a cylindrical cavity with a conical bottom and a conical diaphragm, having the following geometric parameters: aperture radius  $R_0 = 0.5$ , cylindrical part radius  $R_1 = 1$ , cavity length  $Z_3 = 10$ , conical bottom angle  $\chi_1 = 120^\circ$ , and conical diaphragm angle  $\chi_3 = 90^\circ$ . The cavity was made of stainless steel. After a special mechanical treatment that ensured the diffusivities of the bottom and the diaphragm of  $D_1 = D_3 = 0.2$  and of the cylindrical part of  $D_2 = 0.8$  within the wavelength range of 10 to 25  $\mu\text{m}$ , the inner surface of the cavity was oxidized.

The model hemispherical spectral emissivities of the flat specimen of stainless steel for further calculation are shown in Fig. 8 (see, e.g., Ref. 13). The cavity spectral normal effective emissivities were calculated for the following five temperature distributions: first and second, the cavity bottom is isothermal at a temperature of 1000 K, there is a linear decrease in temperature along the cylindrical wall to 980 and 950 K, respectively, and the diaphragm has a

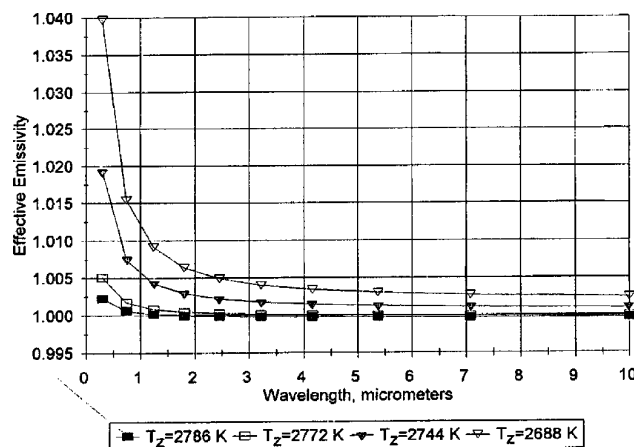


Fig. 6. Spectral normal effective emissivities of a cylindrical cavity for the fifth family of temperature distributions.

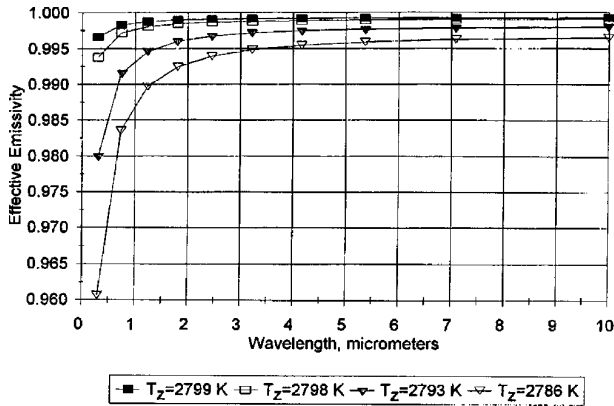


Fig. 7. Spectral normal effective emissivities of a cylindrical cavity for the sixth family of temperature distributions.

constant temperature equal to the cylindrical edge temperature; third through fifth, the bottom center has a temperature of 1000 K, the temperature increases linearly to the periphery of the bottom to 1001, 1002, and 1005 K, respectively, and the cylindrical part and diaphragm of the cavity are at the same constant temperatures. In each of these cases the conical bottom center temperature (equal to 1000 K) was taken as a reference temperature. Results from the calculations are given in Fig. 9. As follows from the results of the calculation, the behavior of  $\epsilon_{en}(\lambda, T_0)$  is mainly determined by  $\lambda$  dependence when the nonisothermality of the cavity walls is negligible. The nonlinear distortions in the short-wave region increase simultaneously with increasing nonisothermality, especially along the visible part of the cavity bottom.

### 6. Reference Temperature Selection

When calculating spectral effective emissivities of nonisothermal cavities, most researchers prefer to take the bottom center temperature as a reference. For some types of temperature distributions, however, such a choice may result in a substantial nonuniformity of the spectral effective emissivity distributions in wavelengths, especially in the short-wave region. This, in turn, results in small wavelength variations that cause significant variations in

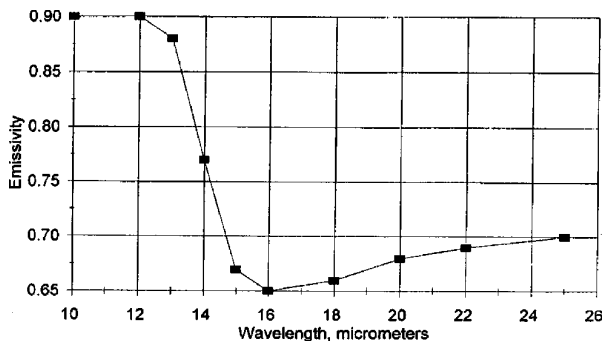


Fig. 8. Spectral hemispherical emissivities of a flat specimen of oxidized stainless steel.

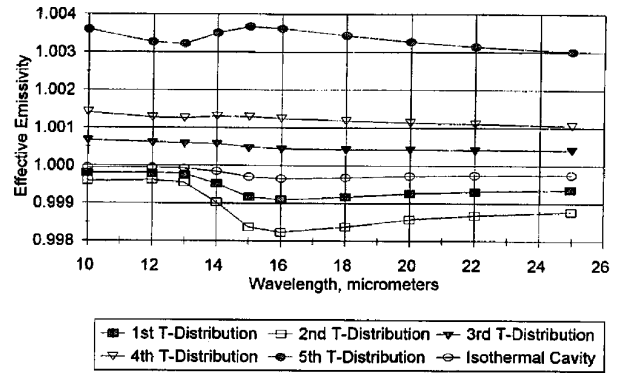


Fig. 9. Spectral normal effective emissivities of a cylindroconical cavity.

effective emissivity, which may cause an increase of errors in some computing operations.

Numerical experiments have been carried out for the cavities discussed in Sections 4 and 5 to investigate the influence of the selected reference temperature on the nature of the dependence,  $\epsilon_{en}(\lambda, T_0)$ . For the cylindrical cavity with a flat bottom and a flat diaphragm, the temperature distribution was modeled by the specification of temperatures at the following points: the bottom center, 2800 K; the bottom periphery, 2797 K; the cylindrical generatrix center, 2744 K; and the diaphragm edge near the aperture, 2744 K. For the cylindrical cavity with a conical bottom and a conical diaphragm, temperatures at the same points were 1000, 1000.5, 990, and 980 K. Temperatures between these points were obtained by means of cubic spline interpolation. Results from the calculations for various reference temperature values are given in Figs. 10 and 11.

The analysis of these results has made it possible to form the following hypothesis. For any nonisothermal cavity with prespecified geometric parameters, wall radiation characteristics, temperature field, and observations, there is a reference temperature,  $T_0^*$ , at which effective emissivities are equal to appropriate values of the same isothermal cavity. This hypothesis was checked by means of numerical experiments for various blackbody cavities and temperature

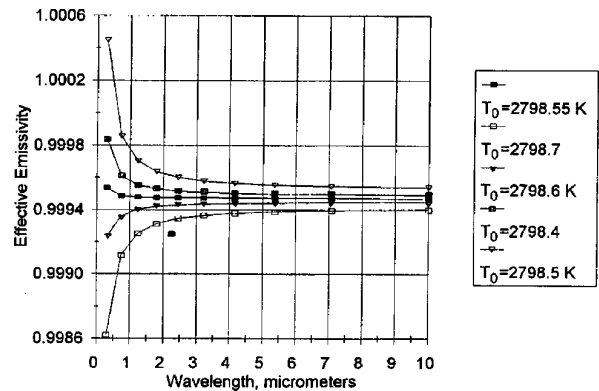


Fig. 10. Spectral normal effective emissivities of a nonisothermal cylindrical cavity for five reference temperatures.

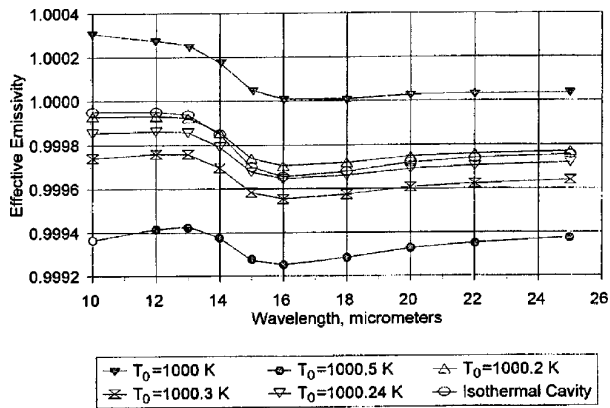


Fig. 11. Spectral normal effective emissivities of a nonisothermal cylindroconical cavity for five reference temperatures.

distributions. Normal, hemispherical, and conical solid-angle-averaged spectral effective emissivities were calculated. In each of the cases, by selecting the reference temperature we managed (within the calculation error) to make the correction for the cavity nonisothermality,  $\Delta\epsilon_e(\lambda, T_0)$ , equal to zero.

The selection of the reference temperature essentially influences the behavior of the spectral effective emissivity as a function of wavelength. The correct selection of the reference temperature allows us to avoid inconvenient values of  $\epsilon_e > 1$  (the arbitrary selection of reference temperature allows us to assign to  $\epsilon_e$  an arbitrary value, from zero to infinity) and allows us to compare the radiative properties of cavity radiators correctly. For each nonisothermal cavity, there is a characteristic reference temperature (call it the optimal reference temperature,  $T_e^*$ ), at which the spectral effective emissivity coincides with that value for the same isothermal cavity. Unambiguous correspondence between the temperature distribution function and the effective reference temperature makes it possible to characterize each temperature distribution by its  $T_e^*$  number instead of by the  $\epsilon_e(\lambda, T_0)$  function with the same spectral effective emissivity of the isothermal cavity,  $\epsilon_e(\lambda)$ .

## 7. Conclusion

The main conclusion from our numerical experiments is as follows. The degree of nonisothermality of that part of the radiating surface that can be observed by the detecting equipment is dominant in the influence on the spectral effective emissivities of the cavity. The more distant the essentially nonisothermal part of the cavity, the lower its influence on the spectral effective emissivity. Therefore, in some cases, the efforts of development engineers to reach isothermality of the whole cavity surface are excessive.

The proposed approach to the selection of reference temperature of the nonisothermal cavities allows us to avoid the uncertainty in its radiation characteristics and to compare the values of effective emissivities

of different blackbody cavities correctly. It is obvious that the optimal reference temperature,  $T_e^*$ , can be represented as a certain surface-averaged value,

$$T_0^* = \frac{1}{S} \int_S T(\xi) Q(\xi) dS, \quad (22)$$

where  $Q(\xi)$  is a weight function specified by the cavity geometry, the cavity wall radiation characteristics, and the observation conditions. Apparently a general form of  $Q(\xi)$  can be indicated *a priori*, at least for diffuse cavities.

The algorithm described above for the calculation of effective emissivities of cavities has demonstrated good accuracy and universalism. The part of the algorithm that realizes random particle walks is easy to modify for the calculation of parameters of cavities of other geometric configurations, including those with self-shadowing surfaces (a reentrant conical bottom, inner partitions), asymmetrical cavities, and the like. The algorithm can also be easily modified for cavities with an arbitrary distribution of optical characteristics on the inner surface.

By specifying the angular distribution of the initial trajectory sections, one can vary cavity observation conditions, calculating the semispherical average in a certain conical solid angle or directional effective emissivities. Only the absence or shortage of experimental data may prevent the development of a model that is closer to reality than the isotropic specular-diffuse cavity to be used for radiation characteristics of the inner walls.

## References

1. Y. Ohwada, "Mathematical proof of an extended Kirchhoff law for a cavity having directional-dependent characteristics," *J. Opt. Soc. Am. A* **5**, 141-145 (1988).
2. R. E. Bedford and C. K. Ma, "Emissivities of diffuse cavities: isothermal and nonisothermal cones and cylinders," *J. Opt. Soc. Am.* **64**, 339-349 (1974).
3. R. E. Bedford and C. K. Ma, "Emissivities of diffuse cavities. II: Isothermal and nonisothermal cylindro-cones," *J. Opt. Soc. Am.* **65**, 565-572 (1975).
4. R. E. Bedford and C. K. Ma, "Emissivities of diffuse cavities. III. Isothermal and nonisothermal double cones," *J. Opt. Soc. Am.* **66**, 724-730 (1976).
5. R. E. Bedford, C. K. Ma, Z. Chu, Y. Sun, and S. Chen, "Emissivities of diffuse cavities. 4. Isothermal and nonisothermal cylindro-inner-cones," *Appl. Opt.* **24**, 2971-2980 (1985).
6. Y. Ohwada, "Evaluation of effective emissivities of nonisothermal cavities," *Appl. Opt.* **22**, 2322-2325 (1983).
7. J. S. Redgrove and K. H. Berry, "Emissivity of a cylindrical blackbody cavity having diffuse and specular components of reflectivity with a correction term for nonisothermal conditions," *High Temp. High Pressures* **15**, 1-11 (1983).
8. F. O. Bartell and W. L. Wolf, "Cavity radiator theory," *Infrared Phys.* **16**, 13-26 (1976).
9. A. Ono, "Calculation of the directional emissivities of cavities by the Monte Carlo method," *J. Opt. Soc. Am.* **70**, 547-554 (1980).

10. R. P. Heinisch, E. M. Sparrow, and N. Shamsundar, "Radiant emission from baffled conical cavities," *J. Opt. Soc. Am.* **63**, 152–158 (1973).
11. V. I. Sapritsky and A. V. Prokhorov, "Calculation of the effective emissivities of specular-diffuse cavities by the Monte Carlo method," *Metrologia* **29**, 9–14 (1992).
12. R. Siegel and J. R. Howell, *Thermal Radiation Heat Transfer*, 2nd ed. (McGraw-Hill, New York, 1981).
13. U. Kienitz, "Infrarot-Strahlungsmeßverfahren zue berührungslosen Bestimmung von Temperature und Oberflächenemissionenseigenschaften," *Wiss. Z. Tech. Univ. Dresden* **35**, 30–32 (1986).